Molecular Biology Reports (2025) 52:1023
https://doi.org/10.1007/s11033-025-11145-3

ORIGINAL ARTICLE

# Microglial NLRP3 inflammasome activation leads to perineuronal net loss in cocultured neurons

**Emre Tarakcioglu**[1,2] · **Kemal Ugur Tufekci**[3,4] · **Sermin Genc**[1,2,5]

Received: 15 May 2025 / Accepted: 6 October 2025
© The Author(s), under exclusive licence to Springer Nature B.V. 2025

## Abstract

**Background** Microglia play a crucial role in maintaining the health of the central nervous system (CNS) through synaptic pruning, debris clearance, and pathogen elimination; however, sustained microglial inflammation can lead to neuronal damage. The NLRP3 inflammasome, a key regulator of inflammatory responses, has been implicated in various CNS diseases. Perineuronal nets (PNNs) are specialized structures that encase neuron somas, protect neurons from oxidative stress, and stabilize synaptic connections. While inflammatory microglia can degrade PNNs, the specific role of inflammasomes in this degradation process remains unclear.

**Methods and results** To investigate the role of inflammasomes in degradation of PNNs, neurons were derived from the murine Neuro-2a cell line using retinoic acid. Subsequently, we induced the NLRP3 inflammasome in the murine N9 microglial cell line via exposure to lipopolysaccharide and ATP. The effect of NLRP3 activation on degradation of PNNs was examined by coculturing neurons and microglia with and without NLRP3 inhibition for 24 h. PNNs were quantified using immunofluorescence staining with Wisteria floribunda agglutinin and neurocan antibodies, both of which bind to PNNs. Our findings demonstrate that coculture with NLRP3-activated microglia reduces the percentage of WFA- and neurocan-positive neurons whereas the inhibition of NLRP3 reverses this effect.

**Conclusions** Our findings highlight the significant role of the NLRP3 inflammasome in the degradation of PNNs in inflammatory states. Moreover, our research suggests that targeting the NLRP3 inflammasome could protect PNN-positive neurons from the damaging effects of inflammation. These findings might provide insight into the inflammatory mechanisms underlying loss of PNNs.

**Clinical trial number** Not applicable.

✉ Sermin Genc
sermin.genc@deu.edu.tr

1 Izmir Biomedicine and Genome Center, Balcova, Izmir, Turkey

2 Izmir International Biomedicine and Genome Institute, Dokuz Eylul University, Izmir, Turkey

3 Center for Brain and Neuroscience Research, Izmir Democracy University, Izmir, Turkey

4 Department of Health Care Services, Vocational School of Health Services, Izmir Democracy University, Izmir, Turkey

5 Department of Neuroscience, Health Sciences Institute, Dokuz Eylul University, Izmir, Turkey

Published online: 13 October 2025

## Graphical abstract

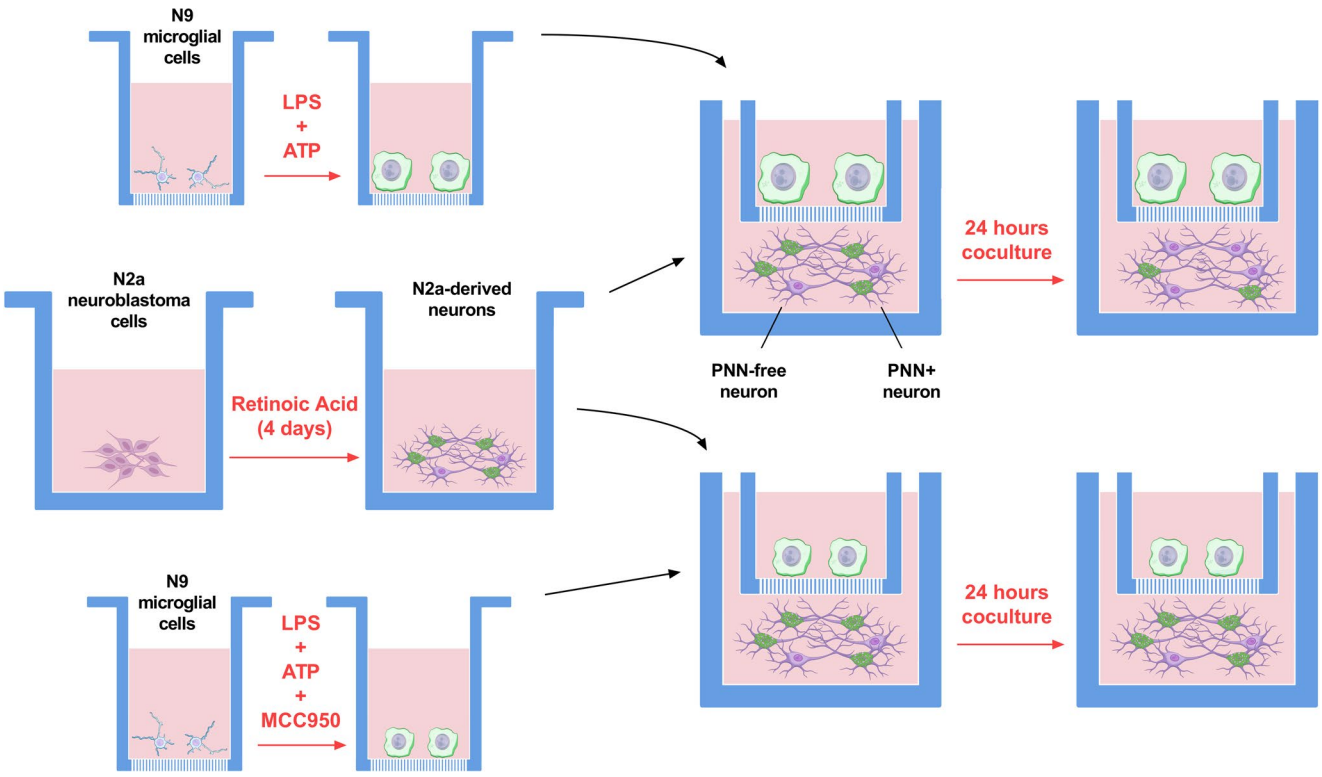


**Keywords** Microglia · Neuron · Perineuronal net · Neuroinflammation · Inflammation

### Abbreviations

| | |
|---|---|
| ATP | Adenosine triphosphate |
| ASC | Apoptosis-associated speck-like protein containing a CARD |
| CNS | Central nervous system |
| CSPG | Chondroitin sulfate proteoglycan |
| GSDMD | Gasdermin-D |
| IL | Interleukin |
| LPS | Lipopolysaccharide |
| N2a | Neuro-2a |
| NLRP3 | NOD-like receptor family pyrin domain containing 3 |
| PNN | Perineuronal net |
| qPCR | Quantitative real-time PCR |
| RA | Retinoic acid |
| SDS-PAGE | Sodium dodecyl sulfate–polyacrylamide gel electrophoresis |
| WFA | Wisteria floribunda agglutinin |

## Introduction

The structural organization of the central nervous system (CNS) is significantly influenced by the neuroglia that support neurons. Among these, microglia play a crucial role in the maintenance and development of neurons in both health and disease [1]. Microglia are responsible for pruning synapses, providing phagocytic activity to eliminate debris surrounding neurons, and removing infiltrating pathogens [2]. Consequently, the innate immune response facilitated by microglia within the brain is essential for removing harmful compounds and organisms. However, persistent chronic inflammation in the brain may result in prolonged microglia activation, thereby damaging the neuronal environment [3].

Inflammasomes are multiprotein complexes that trigger several secretory and inflammatory pathways when they contact specific pathogens or damage-associated molecular patterns [4]. The well-characterized inflammasome NOD-like receptor family pyrin domain containing 3 (NLRP3) is involved in numerous CNS diseases and injuries [5, 6]. NLRP3 can be triggered by several molecular cues, including pathogen-associated molecular patterns, extracellular adenosine triphosphate (ATP), potassium efflux, particle

aggregates, lysosomal or mitochondrial instability, and reactive oxygen species [7, 8]. NLRP3 self-oligomerizes following activation by any of these molecular cues. This oligomerization attracts an adaptor protein known as Apoptosis-associated speck-like protein containing a CARD (ASC). Multiple pro-caspase-1 proteins are recruited by the ASC proteins clustered on the NLRP3 complex, leading to proximity-induced cleavage of pro-caspase-1 into its active form, caspase-1. The pore-forming protein Gasdermin-D (GSDMD) and the inactive forms of the inflammatory cytokines Interleukin (IL)−1β and IL-18 are activated via cleavage by caspase-1. Through pores created by active GSDMD, these inflammatory cell contents are released extracellularly and act in a paracrine fashion [8, 9].

Perineuronal nets (PNNs) are netlike sheaths surrounding the somas of a subset of neurons, especially parvalbumin-positive, GABAergic fast-spiking interneurons [10]. PNNs protect neurons from oxidative stress [11] and stabilize their synaptic connections [10]. The formation and maintenance of PNNs are vital for memory retention (due to their synapse-stabilizing function) [12] and for the protection of the neuron somas from external reactive oxygen species (owing to the antioxidant properties of components of the PNN) [11]. PNNs are composed of various protein- and sugar-based molecules, some of which also appear in extracellular matrices elsewhere in the body. The three major components of PNNs are chains of hyaluronan (a glycosaminoglycan also known as hyaluronic acid); chondroitin sulfate proteoglycans (CSPGs), including aggrecan, brevican, neurocan, and versican; and binding proteins, including Hapln1, Hapln2, Hapln4, and the glycoprotein Tenascin-R [13, 14].

Microglial activation has been demonstrated to induce degradation in PNNs of primary neurons in vitro [15] and in mammal brains in vivo [16]. While there have been studies on inflammation-induced degradation of PNNs in animals and isolated cells, this degradation has not been studied in vitro in cell lines, which are easily maintainable and provide a platform for quickly reproducible tests. It has also not been shown to what extent, if at all, NLRP3 inflammasome activation has a role in microglia-induced degradation of PNNs. In this study, to investigate these unexplored areas, we first examined whether the mouse neuronal cell line Neuro-2a (N2a) expresses PNN-components. After confirming that such components are present in differentiated N2a cells, we cocultured N2a cells with N9 mouse microglial cells both with and without an NLRP3 inhibitor, to determine if inflammation-induced degradation of PNNs can be replicated in vitro and to assess whether NLRP3 plays a significant role in this degradation.

## Materials and methods

### Cell culture

Neuro-2a (N2a) mouse neuroblastoma cell line was purchased from ATCC (Catalog number: CCL-131, RRID: CVCL_0470). N2a cells were cultured in Dulbecco's MEM (DMEM) (ThermoFisher Scientific, 11965084) supplemented with 10% fetal bovine serum (FBS) (ThermoFisher Scientific, 16140071), 2 mM L-glutamine (ThermoFisher Scientific, A2916801), and 100 U/ml penicillin + 100 µg/ml streptomycin (ThermoFisher Scientific, 15140148).

The N9 mouse microglial cell line (RRID: CVCL_0452) was kindly provided by Dr. Paola Ricciardi-Castagnoli (Cellular Pharmacology Center, Milan, Italy) [17]. N9 cells were cultured in RPMI 1640 (ThermoFisher Scientific, 11875093) with 10% FBS, 2 mM L-glutamine, 100 U/ml penicillin, and 100 µg/ml streptomycin. All cells were cultured in incubators at 37 °C with 5% $CO_2$.

### Neuronal differentiation

N2a cells were seeded on poly-D-lysine (PDL) coated glass coverslips placed inside cell culture plates at 18—20 × $10^3$ cells/$cm^2$ for differentiation. For coating, PDL (Sigma-Aldrich, P1149) solution in distilled sterile water was applied at 5 µg/$cm^2$ for 2 hours, then washed two times with distilled sterile water before cell seeding. Differentiation was started one day after seeding, using DMEM containing 1% FBS, 2 mM glutamine, and 10 µM retinoic acid (RA) (Cayman Chemical, 11017), and the medium was changed every two days. For coculture experiments, N2a cells differentiated for four days were used.

### NLRP3 inflammasome activation model

NLRP3 inflammasome activation was induced by treatment with lipopolysaccharide (LPS) for inflammatory priming and ATP for NLRP3 activation, as described previously [18]. N9 microglial cells were seeded at 35—40 × $10^3$ cells/$cm^2$ on cell culture flasks, dishes or 0.4 µm pore-size transparent transwell inserts (Greiner, 662641). The next day, the medium was replaced with RPMI 1640 with 2 mM L-glutamine (without serum or antibiotics).

Cells were divided into the following groups: Control (Ctrl), LPS + ATP (LA), CtrlMCC, and LAMCC (Ctrl and LA groups treated with the NLRP3 inhibitor MCC950). The LPS + groups were treated with LPS (InvivoGen, Ultrapure LPS from *E. Coli* 0111:B4) at a concentration of 1 µg/ml. After 3 h, the MCC + groups were treated with MCC950 (Medchemexpress, HY-12815 A) at a concentration of 0.1 µM. Following a one-hour treatment with MCC950,

the ATP+groups were treated with ATP (Sigma-Aldrich, A6419) at a concentration of 5 mM, and cells were incubated for 1 h. In all groups, previously added molecules were kept at a constant concentration throughout each step.

## N2a-N9 coculture

At the end of the inflammasome activation protocol, plates with N9 transwell inserts were centrifuged at 300 × g for one minute to settle any detached cells. Then, the medium was removed and replaced with DMEM medium containing 1% FBS and 2 mM glutamine. The same medium was applied to N2a cells on day 4 of differentiation after aspiration of the RA-containing medium. After medium replacements, the transwell inserts with N9 cells were placed on the 4-day-differentiated N2a wells using sterile forceps. The coculture system was incubated at 37 °C for 24 h. The cells were used for downstream analyses at the end of 24 h. The neuronal cells in the coculture experiment are divided into five groups: N2a cells cultured alone (termed "noCC/no coculture"), and N2a cells cultured with microglia from the Ctrl, LA, CtrlMCC, and LAMCC groups (with the same group names).

## RNA isolation and quantitative real-time PCR

RNA from cells grown in PDL-coated cover slips inside 24-well plates was isolated using TRI Reagent (Zymo Research, R2050-1–200). For each group, lysates from each well were pooled with lysates from the neighboring well, making a total of 4 samples from 8 wells. Briefly: each sample was lysed in 600 µl of TRI Reagent and vortexed; 120 µl chloroform (Merck-Millipore 1.02445) was added per sample, tubes were shaken vigorously, and tubes were centrifuged at 12,000 × g for 15 min at 4 °C. The aqueous phase was moved to a new tube and mixed with 300 µl isopropanol (ISOLAB, 961.023); then centrifuged at 12,000 × g for 10 min at 4 °C. The supernatant was discarded, and the pellet was resuspended in 600 µl of 75% ethanol (ISOLAB, 920.027) and centrifuged at 7500 × g for 5 min at 4 °C. The supernatant was aspirated, and the pellet was air-dried for 5–10 min. The pellet was dissolved in 25 µl of RNase-free water, and RNA concentration was determined via Nanodrop 2000 (ThermoFisher Scientific).

According to the manufacturer's instructions, cDNA was prepared using the High-Capacity cDNA Reverse Transcription Kit (Applied Biosystems, 4368813). For quantitative real-time PCR (qPCR), Luna Universal qPCR Master Mix was used (New England Biolabs, M3003E) following the manufacturer's instructions, together with Applied Biosystems 7500/7500 Fast Real-Time PCR System. Primers used for the qPCR are listed in Table 1. Relative expression levels were measured by the $2^{-\Delta\Delta ct}$ method [19] with *Gapdh* as the housekeeping gene for normalization.

**Table 1** List of primers used in qPCR

| Primer | Sequence (5' to 3') |
|---|---|
| *Map2* Forward | GCCAGCCTCGGAACAAACA |
| *Map2* Reverse | GCTCAGCGAATGAGGAAGGA |
| *Ncan* Forward | GGGTGTCATTGCCTGCTTATC |
| *Ncan* Reverse | AGCGAAGGTCAGCGCATAG |
| *Rbfox3 (NeuN)* Forward | GCTGAGATTTATGGAGGCTATGC |
| *Rbfpx3 (NeuN)* Reverse | CCGATGGTGTGATGGTAAGGAT |
| *Gapdh* Forward | TGGCCTTCCGTGTTCCTAC |
| *Gapdh* Reverse | GAGTTGCTGTTGAAGTCGCA |

## Immunofluorescent staining

For the detection of PNNs, differentiated N2a cells were fixed with 4% paraformaldehyde in phosphate-buffered saline (PBS)(Biowest, L0615) for 10 min at room temperature and washed three times with PBS. Afterward, the cells were kept at room temperature for one hour with a blocking and permeabilization (block/perm) solution containing 2% FBS and 0.2% Triton-X 100. Subsequently, fluorescein-conjugated *Wisteria floribunda* agglutinin (WFA) (ThermoFisher Scientific, L32481), which targets chondroitin sulfate groups in PNNs, was added to the coverslips (diluted 1:300 in block/perm solution), and the cells were incubated in the dark at 4 °C overnight. For confirmation, in addition to WFA, cells were stained with an antibody for neurocan core protein (Affinity Biosciences Cat# DF4236, RRID: AB_2836587, 1:300 dilution). In both WFA and neurocan staining procedures, MAP2 antibody was used to stain for mature neurons (ThermoFisher Scientific Cat# PA1-10005, RRID: AB_1076848, 1:1000 dilution). The next day, after three PBS washes, Alexa Fluor 488-conjugated anti-rabbit secondary antibody (ThermoFisher Scientific Cat# A-21206, RRID: AB_2535792, diluted 1:800), Alexa Fluor 568-conjugated anti-chicken secondary antibody (ThermoFisher Scientific Cat# A78950, RRID: AB_2921072, diluted 1:1000), and Hoechst 33342 dye for nuclei (AppliChem, A0741, 1 µg/ml) were applied to the cells in the block/perm solution, and the cells were kept in the dark at room temperature for one hour. After three PBS washes, the coverslips were removed from the plates and placed on slides with Prolong Glass mounting medium (ThermoFisher, P36980). After curing, imaging was performed on a confocal microscope (Zeiss LSM 880). Analysis and processing of the images were performed using ImageJ (RRID: SCR_003070), where Hoechst, MAP2, and WFA/Neurocan photographs were merged into a single image. MAP2-positive cells were defined as neurons [20]. Neurons with lattice-like neurocan or WFA staining around the soma were considered "neurocan-positive" or "WFA-positive",

respectively, consistent with previous literature using the same selection criteria [21, 22]. The sample (well) number for each group was three ($n = 3$); three microscope images were acquired from each individual sample; and quantifications were performed in each image. In comparisons between groups, the ratios of neurocan- or WFA-positive neurons to total neurons were used.

### Western blot

At the end of the inflammasome activation protocol, cells were scraped and centrifuged at 500 × g. To determine levels of released caspase-1 and IL-1β, the supernatants (cell media) after centrifugation were moved into separate tubes, lyophilized, and dissolved in RIPA + inhibitor cocktail. The remaining cell pellets were lysed with RIPA cell lysis buffer (ThermoFisher Scientific 89900) with 1% Halt Protease and Phosphatase Inhibitor Cocktail (ThermoFisher Scientific 78447). Lysed cells were vortexed on ice for 30 min and centrifuged at 12,000 × g. The supernatants of lysed pellets were stored at −80 °C for immunoblotting. Protein concentrations of lysates and supernatants were measured using the BCA Protein Colorimetric Assay Kit (Elabscience E-BC-K318-M).

The proteins were then separated by SDS-PAGE, transferred from the gel to polyvinylidene difluoride membranes, and blocked in Tris-buffered saline with 0.01% Tween-20 (TBST) with 3% milk. After blocking, the membranes were incubated with antibodies recognizing NLRP3, actin, caspase-1 and IL-1β proteins (respectively: AdipoGen Cat# AG-20B-0014, RRID: AB_2490202, diluted 1:800 in 3% bovine serum albumin (BSA); Cell Signaling Technology Cat# 8457, RRID: AB_10950489, diluted 1:1000 in 3% BSA; AdipoGen Cat# AG-20B-0042, RRID: AB_2490248, diluted 1:400 in 1% milk; Abcam Cat# ab9722, RRID: AB_308765, diluted 1:400 in 1% milk) overnight. After three washes with TBST, 1 h incubation with compatible secondary antibodies conjugated with horseradish peroxidase (for mouse and rabbit IgGs, respectively: Cell Signaling Technology Cat# 7076, RRID: AB_330924; Jackson ImmunoResearch Labs Cat# 111-035-144, RRID: AB_2307391; both diluted 1:1000 in 3% milk), and three more washes with TBST, the membranes were imaged using a chemiluminescent solution (ThermoFisher Scientific 34577), using ChemiDoc MP Imaging System (Bio-Rad). The intensity analyses of the protein bands were performed in the Image Studio Lite software (LI-COR Biosciences, RRID: SCR_013715). Actin bands were used as loading controls for normalizing the NLRP3 bands.

### Statistical analyses

Statistical analyses and their graphical representations were performed in GraphPad Prism (version 8, RRID: SCR_002798). Data are presented as mean ± standard error of mean (SEM). Normality of the data was assessed using the Shapiro–Wilk test. Comparisons between two groups where both distributions are normal were analyzed using the Student's t-test. Comparisons between two groups with at least one non-normal distribution were analyzed with the Mann–Whitney U-test. Comparisons between multiple groups were analyzed using ANOVA with the Bonferroni multiple comparisons test. Comparisons between multiple non-normal distribution groups were analyzed using the Kruskal-Wallis test with Dunn's multiple comparisons test. The threshold for statistical significance was set at $p < 0.05$.

## Results

### Differentiation of N2a cells into PNN-positive neurons

In order to determine the presence of PNNs in neurons in vitro, we first set out to establish a model of neuronal differentiation in the mouse N2a neuroblastoma cell line. The cells were incubated with 10 µM RA for 3 and 4 days to induce neuronal differentiation. Analysis of RNA expression during this differentiation period revealed that the mature neuron markers *Map2* and *Rbfox3* (NeuN) increased on days 3 and 4 compared to undifferentiated cells (Fig. 1a, b). We examined when *Ncan*, which codes for the protein neurocan (a component of PNNs), showed increased mRNA levels and found significant upregulation on days 3 and 4 (Fig. 1c).

To further probe whether PNNs were present in differentiated N2a cells, we performed immunostaining with WFA-fluorescein (which binds to CSPGs of PNNs) and neurocan antibody on undifferentiated N2a cells and cells at day 4 of differentiation, using MAP2 antibody to stain for neurons. The immunofluorescence images showed a rise in WFA- and neurocan-positive neurons on day 4 compared to day 0 (Fig. 2). Considering the substantial increase in mature neuron markers, *Ncan* mRNA expression, and PNN-component staining at day 4, it was chosen as the starting time point for our coculture model.

### Coculture of neurons with inflammasome-activated microglial cells

To attain NLRP3 inflammasome activation in N9 microglial cells, we incubated the cells in a serum-free medium with

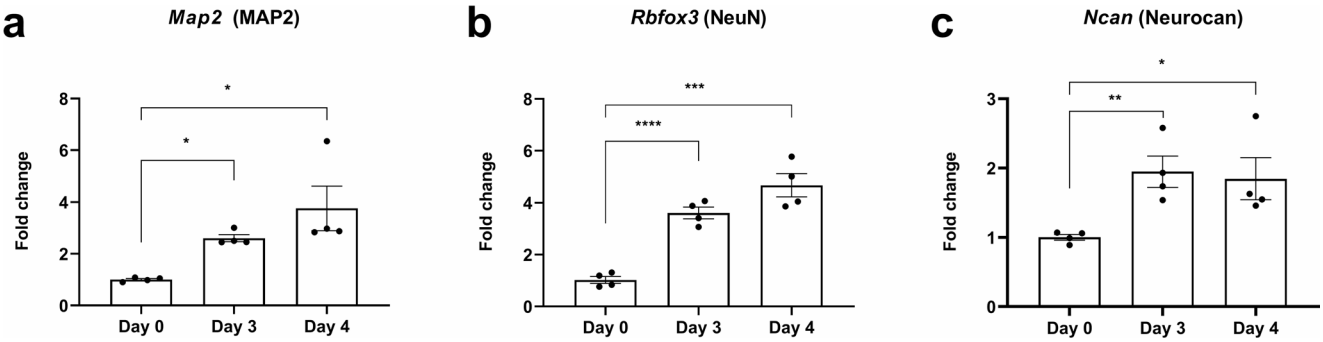


**Fig. 1** mRNA expression of neuronal markers and neurocan increases with RA treatment in N2a cells. Changes in mRNA expression of *Map2* (**a**), *Rbfox3* (NeuN) (**b**), and *Ncan (*Neurocan*)* (**c**) in N2a cells at day 0, 3, and 4 of 10 µM RA treatment. Relative expression levels are measured via the $2^{-\Delta\Delta ct}$ method with *Gapdh* as the housekeeping gene for normalization. ($n=4$; * = $p<0.05$; ** = $p<0.01$; **** = $p<0.0001$ compared to Day 0; data are presented as mean ± SEM; data for *Map2* and *Ncan* data were analyzed using the Kruskal-Wallis test with multiple comparisons and data for *Rbfox3* were analyzed using ANOVA with multiple comparisons.)

LPS and then ATP (with and without the NLRP3 inhibitor MCC950). At the end of the model (after 1 h incubation with ATP), the microglial cells were transferred into coculture with differentiated N2a cells and incubated for 24 h (Fig. 3a). To confirm the inflammasome model and efficacy of the inhibitor, the same experimental setup was performed separately on culture flasks and analysed via immunoblotting. The inflammasome model induced an increase in NLRP3 (in cell homogenates), cleaved IL-1β, and cleaved caspase-1 (in cell media) in the LA group. The rise in IL-1β and caspase-1 was reversed in the LAMCC group, suggesting that NLRP3 activation was successfully inhibited by MCC950 (Fig. 3b, d, e). The NLRP3 protein levels in the LAMCC group were similar to the levels in the LA group, both being upregulated as a result of LPS treatment [23] (Fig. 3b, c). This stability in NLRP3 protein levels was expected since MCC950 is reported to inhibit only the assembly of the NLRP3 inflammasome and not affect NLRP3 protein levels [24]. The microglial cells were also imaged at the end of the inflammasome activation model via phase contrast microscopy, and cells in the LA group were found to be significantly higher in surface area than cells in the other groups. Both LA and LAMCC groups included enlarged cells compared to groups without LPS + ATP treatment, but the average cell size was significantly higher in LA than in LAMCC (Fig. S1a, b). While there were no significant differences between cell numbers except between LA and CtrlMCC, the percentage of dead cells (as identified by propidium iodide staining) in the LA group was significantly higher compared to all other groups (Fig. S1c, d,e).

At the end of the coculture period, PNNs were imaged using WFA-Fluorescein, and WFA-positive cells were counted. There was a reduction in the percentage of WFA-positive neurons in the LA group, while this number remained higher across all other groups (Fig. 4a, b). The experiment was repeated to stain neurocan, a major CSPG in PNNs. This staining showed a similar trend where only the LA group had a significantly lower neurocan-positive neuron number (Fig. 4c, d). Moreover, there were no significant differences between groups for neuron percentages, neuronal surface coverage, or apoptotic cells (Fig. S2, S3, S4), suggesting that neuron numbers were comparable between groups and that there was no major effect of cell death. Thus, NLRP3 inhibition in microglia cocultured with neurons reversed the reduction in WFA- or neurocan-positive neurons.

## Discussion

In this study, we have shown for the first time that the N2a cell line produces components of PNNs (neurocan and chondroitin sulfate proteoglycans that bind WFA) and that these components are upregulated as the cells are exposed to RA and neuronal differentiation takes place. We have also shown that microglia with activated NLRP3 inflammasomes, when cocultured with differentiated N2a cells, lead to a reduction in the number of PNN-positive neurons (i.e., both neurocan-positive and WFA-positive neurons). Furthermore, we have also shown that the NLRP3 inhibition reverses this effect and, consequently, that NLRP3 inflammasome plays a significant role in the degradation of PNNs by activated microglia.

NLRP3 inflammasome activation has been linked to upregulation of several matrix metalloproteinases (MMPs), such as MMP-2 [25] and MMP-13 [26], which may be associated with the degradation of PNNs. In fact, it was shown in mouse knee cartilage that an increase in IL-1β, an indicator of inflammasome activation, was concomitant with MMP-13 increase and aggrecan decrease [26]. Moreover, cathepsins are also implicated in NLRP3 inflammasome activation [27], and neurocan was previously reported to be degraded

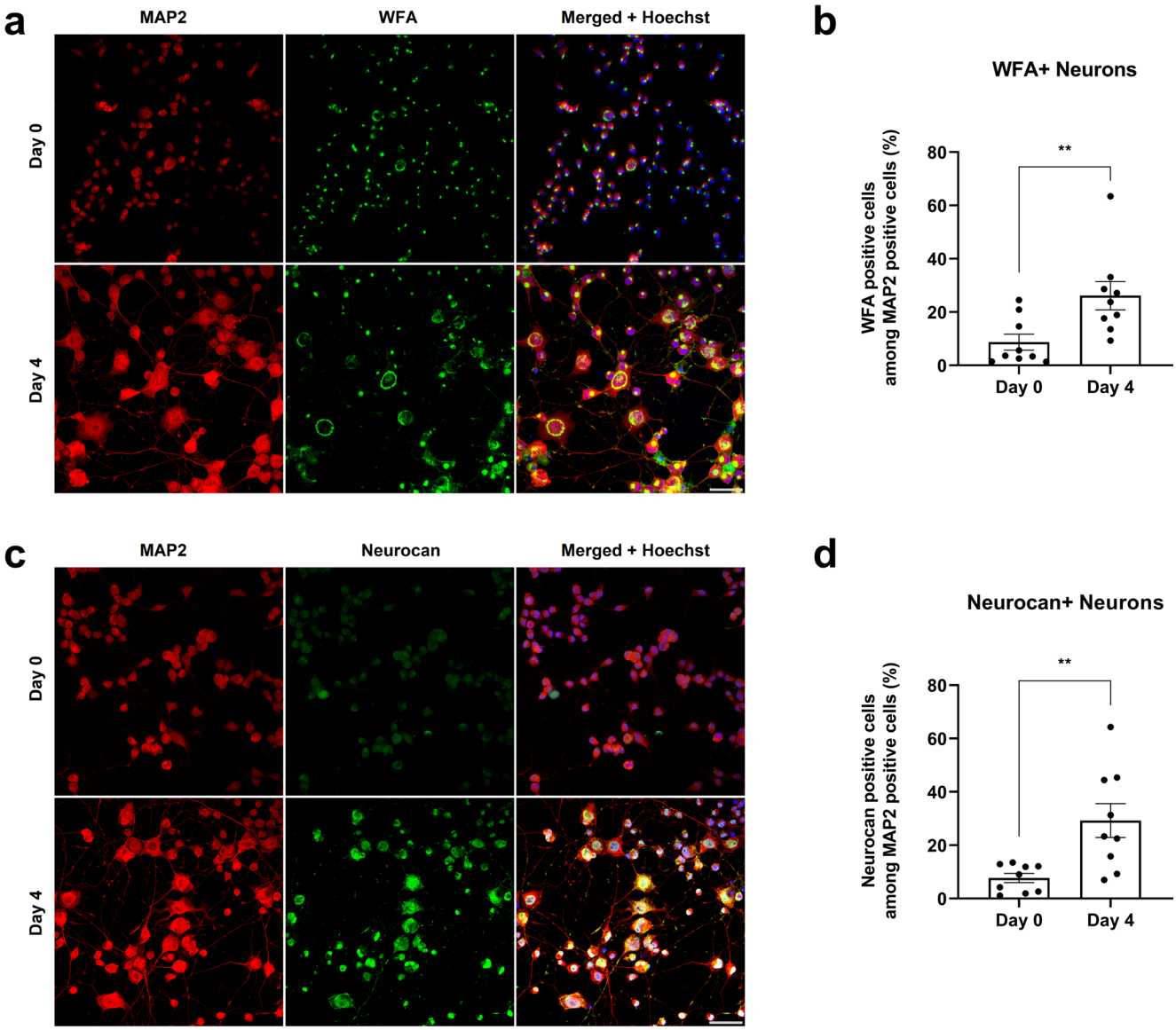


**Fig. 2** WFA-positive and neurocan-positive neurons increase with RA treatment. (**a**) Representative confocal microscopy images of WFA (green) and MAP2 (red) staining in N2a cells at Day 0 and 4 of 10 µM RA treatment (**b**) Percentages of WFA-positive neurons among all cells (**c**) Representative confocal microscopy images of neurocan (green) and MAP2 (red) staining in N2a cells at Day 0 and 4 of 10 µM RA treatment (**d**) Percentages of neurocan-positive neurons among all cells (Scale bar = 50 µm; $n = 3$; three images analysed per sample; * = $p < 0.05$ compared to Day 0; data are presented as mean ± SEM; data for the WFA graph were analyzed using the Mann–Whitney U-test, data for the neurocan graph were analyzed with Student's t-test)

by cathepsin S in rats [28]. Thus, in our coculture, MMPs or cathepsins released from microglial cells might also be responsible for the degradation of PNNs of N2a cells.

Another mechanism through which NLRP3 activation might reduce PNNs is by initiating neuronal cell death. It is observed in our coculture images that neurons cultured with LA microglia have a slightly different morphology with reduced neurite length, suggesting the possibility of changes in the cytoskeleton associated with apoptosis [29]. Previous studies show that microglial-neuronal coculture can lead to neuronal cell death, both with transwell insert systems and in direct coculture systems [30, 31]. Considering the roles of active caspases in different types of cell death [32], our coculture model may involve a degree of microglia-mediated apoptosis, or possibly pyroptosis [33], as well. In our analysis, a count of apoptotic N2a nuclei showed no significant differences in apoptotic cell percentages between groups (**Fig. S4**). However, this method is limited to detecting apoptosis-associated nuclear condensation and fragmentation, and may therefore fail to identify all apoptotic cells. Given the potential overlap between mechanisms, future studies could investigate the interplay between

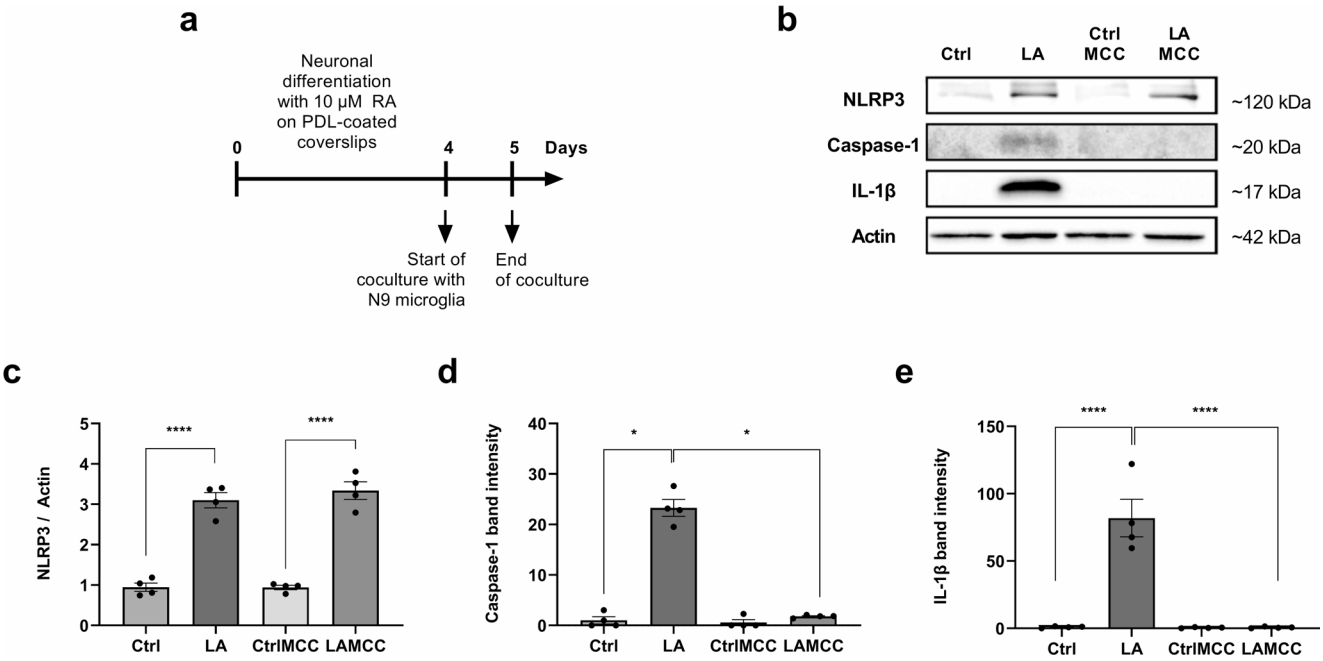


**Fig. 3** Proteins downstream of the NLRP3 inflammasome are increased with LPS+ATP treatment, and the increase is reversed with MCC950 treatment in N9 cells. (**a**) Timeline of the N2a differentiation and N2a-N9 coculture procedure (**b**) Representative western blot bands from the immunoblotting analyses for NLRP3, caspase-1 and IL-1β (**c**) Normalized band intensity for NLRP3 in N9 lysates (**d**) Band intensity quantification of mature caspase-1 in N9 cell media (**e**) Band intensity quantification of mature IL-1β in N9 cell media (Ctrl: Control, LA: LPS+ATP, CtrlMCC: Ctrl+MCC950, LAMCC: LA+MCC950) ($n=4$; * = $p<0.05$; data are presented as mean ± SEM; data for NLRP3 and IL-1β were analyzed using ANOVA with multiple comparisons and data for caspase-1 were analysed using the Kruskal-Wallis test with multiple comparisons

loss of PNNs and neuronal cell death in a more thorough manner to get a fuller picture.

In addition to the deleterious role in the degradation of PNNs observed in our study, microglia also have a neuroprotective function against excitotoxicity. It has been shown that after excessive neuronal stimulation or brain injury, microglia can protect neurons against excitotoxicity and cell death by directly contacting them [34, 35]. CSPGs have similarly been shown to protect neurons against glutamate excitotoxicity [36]. Thus, both microglia and PNNs can contribute to maintaining neuronal survival under excitotoxic conditions. It remains to be determined whether NLRP3 inhibition in microglia under inflammatory conditions influences neuronal function and excitability.

Although this is the first study to demonstrate the effect of the NLRP3 inflammasome on PNNs in vitro, a previous study by our group revealed a similar effect in mouse brains. The in vivo study showed that neonatal LPS injection led to a reduction of PNNs in the hippocampi and cortices of mice in early adulthood, whereas NLRP3 knockout mice injected with LPS were resistant to this reduction [37].

While we have demonstrated a visible link between NLRP3 inflammasome activation and reduction in PNNs of neuronal cells, our study has several limitations. Firstly, PNNs in the brain are created and maintained in an environment where glial cells are present. As our culture model does not include astrocytes or oligodendrocytes, the NLRP3-induced degradation effect might not necessarily translate to the brain, where astrocytes would be communicating with both the neurons and the microglia. It is also possible that astrocytes might exacerbate the effect, as they are also known to express metalloproteinases [38]. A second limitation is that, due to its affinity for chondroitin sulfate groups, WFA might stain more than extracellular chondroitin sulfates. This intracellular staining is visible in some cells characterized by high-intensity WFA-stained circles at the perimeter of the nucleus. It is possible that nuclear perlecan, a proteoglycan that can also have chondroitin sulfate side chains [39, 40], is stained by WFA. A recent study on the spinal innervation of the colon has revealed similar staining patterns for WFA in mice, where neurons with only perinuclear WFA staining appear [41]. The authors of the study note the presence of these structures but have not investigated further into their origins. While the nature of these intracellular WFA targets remains unclear, it is possible that in some neurons, the assembly of glycosaminoglycans into a net-like structure begins inside the cytoplasm. This intracellular staining might also explain the singular high-intensity WFA specks observed in some cells in our study. Such dot-like reactivity has been seen previously in

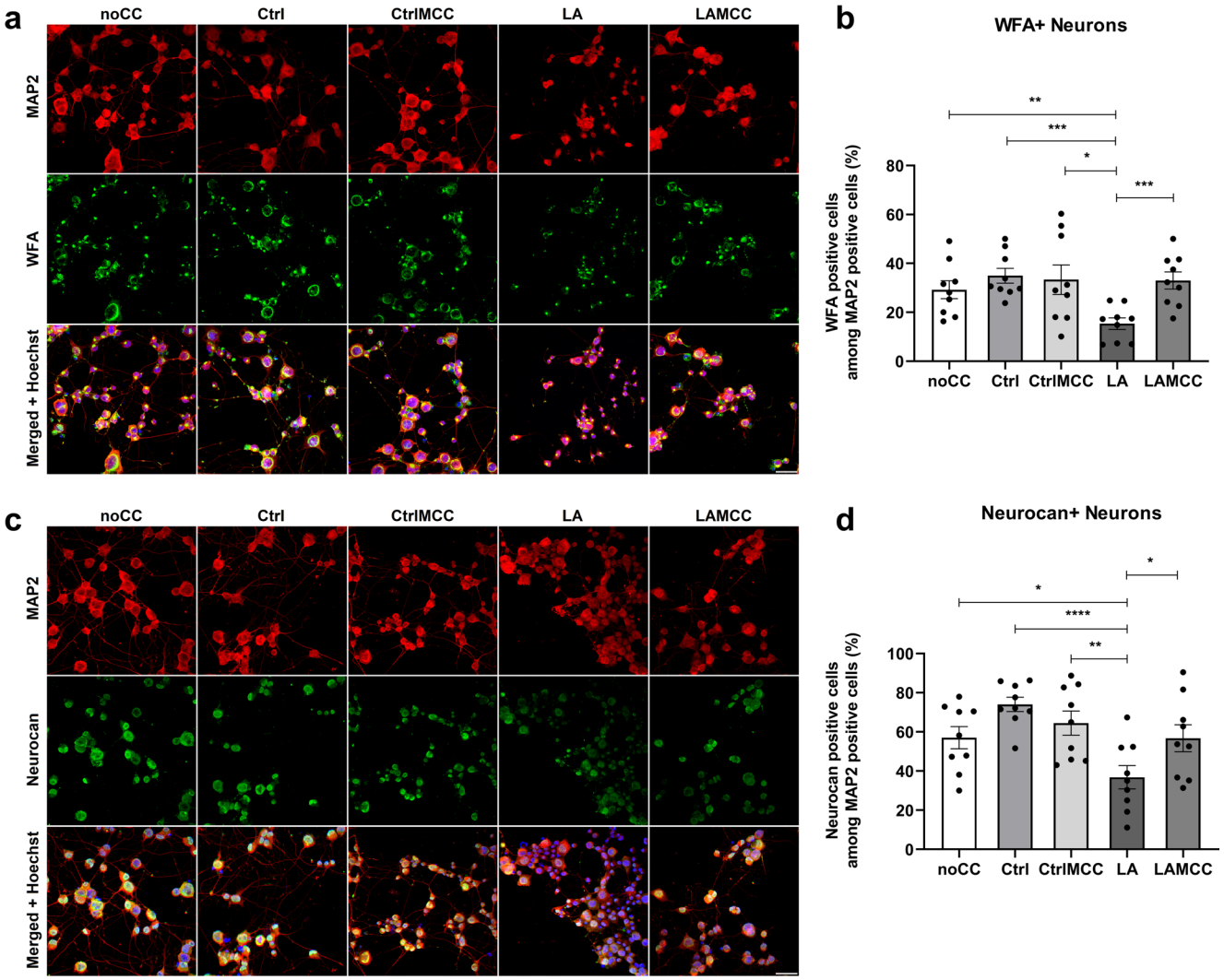


**Fig. 4** The percentages of WFA-positive and neurocan-positive neurons are reduced after coculture with LA microglia, but not with Ctrl, CtrlMCC, or LAMCC microglia. (**a**) Representative confocal microscopy images of WFA (green) and MAP2 (red) staining in N2a cells at the end of the coculture period. (**b**) Quantification of the percentages of WFA-positive neurons among all neurons. (**c**) Representative confocal microscopy images of neurocan (green) and MAP2 (red) staining in N2a cells at the end of the coculture period. (**d**) Quantification of the percentages of neurocan-positive neurons among all neurons. (noCC: No coculture, Ctrl/CtrlMCC/LA/LAMCC: cocultured with Ctrl/CtrlMCC/LA/LAMCC microglia) (Scale bar = 50 µm; $n = 3$; three images analysed per sample; * = $p < 0.05$; ** = $p < 0.01$; *** = $p < 0.001$; data are presented as mean ± SEM; data for all graphs were analysed using ANOVA with multiple comparisons)

staining of mouse brain sections for chondroitin sulfate, where authors considered them to be false positives [42]. Since neither of these unusual structures covered the cell soma, we have not considered them as part of PNNs, and cells that have these staining patterns were only regarded as WFA-positive if they also had WFA staining covering the cell soma. Thirdly, there appears to be a gap between the percentage of WFA and neurocan-positive neurons in our in vitro model: neurocan-positive neurons are more abundant than WFA-positive neurons in both differentiation and coculture models. The variability of components between PNNs of individual cells and the higher affinity of WFA to certain CSPGs might explain this. For example, it is reported that neurons of aggrecan-knockout mice do not stain positively for WFA while still staining positively for other components of PNNs [43].

## Conclusion

Our data indicate that soluble molecules, such as proteins, released from NLRP3-activated microglia induce a reduction in PNN-positive neurons in a microglia-neuron coculture model. This suggests that in acute neuroinflammation caused by microglial activation, drugs directly targeting NLRP3 could prevent PNN degradation. Such an approach

could prevent PNNs from inflammation-associated damage without relying on broad anti-inflammatory drugs like NSAIDs or steroids, which can cause side effects at high doses.

**Supplementary Information** The online version contains supplementary material available at https://doi.org/10.1007/s11033-025-11145-3.

**Acknowledgements** The cell drawings used in the graphical abstract were adapted from images uploaded on SciDraw (scidraw.io) with Creative Commons license.

**Author contributions** All authors contributed to the study conception and design. Material preparation, experimental procedures and analysis were performed by ET. The first draft of the manuscript was written by ET, and all authors commented on and revised all drafts. All authors read and approved the final manuscript.

**Funding** This study was funded by the Dokuz Eylül University Scientific Research Projects Coordination Unit under grant code FDK-2022-2701.

**Data availability** The data in the study are available upon request to the corresponding author.

## Declarations

**Conflict of interest** The authors have no competing interests to declare regarding this article.

**Ethical approval** This study has been approved by the Izmir Biomedicine and Genome Center Non-Interventional Research Ethics Committee with the protocol number 2021-016.

**Consent to participate** Not applicable.

**Consent to publish** Not applicable.

## References

1. Crapser JD, Arreola MA, Tsourmas KI, Green KN (2021) Microglia as hackers of the matrix: sculpting synapses and the extracellular space. Cell Mol Immunol 18:2472–2488. https://doi.org/10.1038/s41423-021-00751-3
2. Guo L, Choi S, Bikkannavar P, Cordeiro MF (2022) Microglia: key players in retinal ageing and neurodegeneration. Front Cell Neurosci 16:804782. https://doi.org/10.3389/fncel.2022.804782
3. Bachiller S, Jimenez-Ferrer I, Paulus A, Yang Y, Swanberg M, Deierborg T, Boza-Serrano A (2018) Microglia in neurological diseases: a road map to brain-disease dependent-inflammatory response. Front Cell Neurosci 12:488. https://doi.org/10.3389/fncel.2018.00488
4. Santoni G, Cardinali C, Morelli MB, Santoni M, Nabissi M, Amantini C (2015) Danger- and pathogen-associated molecular patterns recognition by pattern-recognition receptors and ion channels of the transient receptor potential family triggers the inflammasome activation in immune cells and sensory neurons. J Neuroinflammation 12:21. https://doi.org/10.1186/s12974-015-0239-2
5. Wang L, Hauenstein AV (2020) The NLRP3 inflammasome: mechanism of action, role in disease and therapies. Mol Aspects Med 76:100889. https://doi.org/10.1016/j.mam.2020.100889
6. Eren E, Ozoren N (2019) The NLRP3 inflammasome: a new player in neurological diseases. Turk J Biol 43:349–359. https://doi.org/10.3906/biy-1909-31
7. Latz E, Xiao TS, Stutz A (2013) Activation and regulation of the inflammasomes. Nat Rev Immunol 13:397–411. https://doi.org/10.1038/nri3452
8. Jo EK, Kim JK, Shin DM, Sasakawa C (2016) Molecular mechanisms regulating NLRP3 inflammasome activation. Cell Mol Immunol 13:148–159. https://doi.org/10.1038/cmi.2015.95
9. Voet S, Srinivasan S, Lamkanfi M, van Loo G (2019) Inflammasomes in neuroinflammatory and neurodegenerative diseases. EMBO Mol Med. https://doi.org/10.15252/emmm.201810248
10. Kwok JC, Dick G, Wang D, Fawcett JW (2011) Extracellular matrix and perineuronal nets in CNS repair. Dev Neurobiol 71:1073–1089. https://doi.org/10.1002/dneu.20974
11. Cabungcal JH, Steullet P, Morishita H, Kraftsik R, Cuenod M, Hensch TK, Do KQ (2013) Perineuronal nets protect fast-spiking interneurons against oxidative stress. Proc Natl Acad Sci U S A 110:9130–9135. https://doi.org/10.1073/pnas.1300454110
12. Carulli D et al (2020) Cerebellar plasticity and associative memories are controlled by perineuronal Nets. Proc Natl Acad Sci U S A 117:6855–6865. https://doi.org/10.1073/pnas.1916163117
13. Reichelt AC, Hare DJ, Bussey TJ, Saksida LM (2019) Perineuronal nets: Plasticity, Protection, and therapeutic potential. Trends Neurosci 42:458–470. https://doi.org/10.1016/j.tins.2019.04.003
14. Bosiacki M, Gassowska-Dobrowolska M, Kojder K, Fabianska M, Jezewski D, Gutowska I, Lubkowska A (2019) Perineuronal Nets and their role in synaptic homeostasis. Int J Mol Sci 20. https://doi.org/10.3390/ijms20174108
15. Wegrzyn D, Freund N, Faissner A, Juckel G (2021) Poly I:C activated microglia disrupt perineuronal nets and modulate synaptic balance in primary hippocampal neurons *in vitro*. Front Synaptic Neurosci 13:637549. https://doi.org/10.3389/fnsyn.2021.637549
16. Crapser JD, Spangenberg EE, Barahona RA, Arreola MA, Hohsfield LA, Green KN (2020) Microglia facilitate loss of perineuronal Nets in the alzheimer's disease brain. EBioMedicine 58:102919. https://doi.org/10.1016/j.ebiom.2020.102919
17. Righi M, Mori L, De Libero G, Sironi M, Biondi A, Mantovani A, Donini SD, Ricciardi-Castagnoli P (1989) Monokine production by microglial cell clones. Eur J Immunol 19:1443–1448. https://doi.org/10.1002/eji.1830190815
18. Olcum M, Tufekci KU, Durur DY, Tastan B, Gokbayrak IN, Genc K, Genc S (2021) Ethyl pyruvate attenuates microglial NLRP3 inflammasome activation via Inhibition of HMGB1/NF-kappaB/miR-223 signaling. Antioxid (Basel) 10. https://doi.org/10.3390/antiox10050745
19. Livak KJ, Schmittgen TD (2001) Analysis of relative gene expression data using real-time quantitative PCR and the 2(-Delta delta C(T)) method. Methods 25:402–408. https://doi.org/10.1006/meth.2001.1262
20. Soltani MH, Pichardo R, Song Z, Sangha N, Camacho F, Satyamoorthy K, Sangueza OP, Setaluri V (2005) Microtubule-associated protein 2, a marker of neuronal differentiation, induces mitotic defects, inhibits growth of melanoma cells, and predicts metastatic potential of cutaneous melanoma. Am J Pathol 166:1841–1850. https://doi.org/10.1016/S0002-9440(10)62493-5
21. Haunso A, Ibrahim M, Bartsch U, Letiembre M, Celio MR, Menoud P (2000) Morphology of perineuronal Nets in tenascin-R and parvalbumin single and double knockout mice. Brain Res 864:142–145. https://doi.org/10.1016/s0006-8993(00)02173-9
22. Venturino A et al (2021) Microglia enable mature perineuronal nets disassembly upon anesthetic ketamine exposure or 60-Hz

light entrainment in the healthy brain. Cell Rep. https://doi.org/10.1016/J.Celrep.2021.109313
23. Han S et al (2015) Lipopolysaccharide primes the NALP3 inflammasome by inhibiting its ubiquitination and degradation mediated by the SCFFBXL2 E3 ligase. J Biol Chem 290:18124–18133. https://doi.org/10.1074/jbc.M115.645549
24. Coll RC et al (2015) A small-molecule inhibitor of the NLRP3 inflammasome for the treatment of inflammatory diseases. Nat Med 21:248–255. https://doi.org/10.1038/nm.3806
25. Unamuno X et al (2021) NLRP3 inflammasome Blockade reduces adipose tissue inflammation and extracellular matrix remodeling. Cell Mol Immunol 18:1045–1057. https://doi.org/10.1038/s41423-019-0296-z
26. Liu B et al (2023) Betulinic acid attenuates osteoarthritis via limiting NLRP3 inflammasome activation to decrease Interleukin-1beta maturation and secretion. 3706421. https://doi.org/10.1155/2023/3706421. Mediators Inflamm 2023:
27. Campden RI, Zhang Y (2019) The role of lysosomal cysteine cathepsins in NLRP3 inflammasome activation. Arch Biochem Biophys 670:32–42. https://doi.org/10.1016/j.abb.2019.02.015
28. Petanceska S, Canoll P, Devi LA (1996) Expression of rat cathepsin S in phagocytic cells. J Biol Chem 271:4403–4409. https://doi.org/10.1074/jbc.271.8.4403
29. Desouza M, Gunning PW, Stehn JR (2012) The actin cytoskeleton as a sensor and mediator of apoptosis. Bioarchitecture 2:75–87. https://doi.org/10.4161/bioa.20975
30. Eren E, Tufekci KU, Isci KB, Tastan B, Genc K, Genc S (2018) Sulforaphane inhibits Lipopolysaccharide-Induced Inflammation, Cytotoxicity, oxidative Stress, and miR-155 expression and switches to mox phenotype through activating extracellular Signal-Regulated kinase 1/2-Nuclear factor erythroid 2-Related factor 2/Antioxidant response element pathway in murine microglial cells. Front Immunol 9:36. https://doi.org/10.3389/fimmu.2018.00036
31. Gibbons HM, Dragunow M (2006) Microglia induce neural cell death via a proximity-dependent mechanism involving nitric oxide. Brain Res 1084:1–15. https://doi.org/10.1016/j.brainres.2006.02.032
32. Shalini S, Dorstyn L, Dawar S, Kumar S (2015) Old, new and emerging functions of caspases. Cell Death Differ 22:526–539. https://doi.org/10.1038/cdd.2014.216
33. Han YH, Liu XD, Jin MH, Sun HN, Kwon T (2023) Role of NLRP3 inflammasome-mediated neuronal pyroptosis and neuroinflammation in neurodegenerative diseases. Inflamm Res 72:1839–1859. https://doi.org/10.1007/s00011-023-01790-4
34. Szalay G et al (2016) Microglia protect against brain injury and their selective elimination dysregulates neuronal network activity after stroke. Nat Commun 7:11499. https://doi.org/10.1038/ncomms11499
35. Kato G et al (2016) Microglial contact prevents excess depolarization and rescues neurons from excitotoxicity. eNeuro. https://doi.org/10.1523/ENEURO.0004-16.2016
36. Okamoto M, Mori S, Endo H (1994) A protective action of chondroitin sulfate proteoglycans against neuronal cell death induced by glutamate. Brain Res 637:57–67. https://doi.org/10.1016/0006-8993(94)91217-3
37. Tarakcioglu E, Genc B, Tufekci KU, Genc S (2025) Neonatal NLRP3 inflammasome activation leads to perineuronal net deficits in early adulthood. Dev Neurobiol 85:e22986. https://doi.org/10.1002/dneu.22986
38. Liu LR, Liu JC, Bao JS, Bai QQ, Wang GQ (2020) Interaction of microglia and astrocytes in the neurovascular unit. Front Immunol 11:1024. https://doi.org/10.3389/fimmu.2020.01024
39. Hayes AJ, Melrose J (2021) What are the potential roles of nuclear perlecan and other heparan sulphate proteoglycans in the normal and malignant phenotype. Int J Mol Sci. https://doi.org/10.3390/ijms22094415
40. Gomes R, Kirn-Safran C, Farach-Carson MC, Carson DD (2002) Perlecan: an important component of the cartilage pericellular matrix. J Musculoskelet Neuronal Interact 2:511–516
41. da Silva MDV et al (2024) Perineuronal net in the extrinsic innervation of the distal colon of mice and its remodeling in ulcerative colitis. J Neurochem 168:1937–1955. https://doi.org/10.1111/jnc.16080
42. Horii-Hayashi N, Sasagawa T, Matsunaga W, Nishi M (2015) Development and structural variety of the chondroitin sulfate Proteoglycans-Contained extracellular matrix in the mouse brain. 256389. https://doi.org/10.1155/2015/256389. Neural Plast 2015:
43. Giamanco KA, Morawski M, Matthews RT (2010) Perineuronal net formation and structure in Aggrecan knockout mice. Neuroscience 170:1314–1327. https://doi.org/10.1016/j.neuroscience.2010.08.032

**Publisher's note** Springer Nature remains neutral with regard to jurisdictional claims in published maps and institutional affiliations.

Springer Nature or its licensor (e.g. a society or other partner) holds exclusive rights to this article under a publishing agreement with the author(s) or other rightsholder(s); author self-archiving of the accepted manuscript version of this article is solely governed by the terms of such publishing agreement and applicable law.